IEEE Access
Multidisciplinary | Rapid Review | Open Access Journal

Received December 9, 2020, accepted December 21, 2020, date of publication January 4, 2021, date of current version January 13, 2021.

Digital Object Identifier 10.1109/ACCESS.2020.3049058

Vertically Polarized Quasi-Yagi MIMO Antenna for 5G N78 Band Application

YIZHEN XU[1], (Graduate Student Member, IEEE), YUANDAN DONG[1,2], (Senior Member, IEEE), SICHAO WEN[1], AND HAILONG WANG[2]

[1]School of Electronic Engineering, University of Electronic Science and Technology of China, Chengdu 611731, China
[2]Sichuan Province Engineering Research Center for Broadband Microwave Circuit with High Density Integration, Chengdu 610036, China

Corresponding author: Yuandan Dong (ydong@uestc.edu.cn)

ABSTRACT In this study, a three-port vertically polarized Quasi-Yagi Multiple-Input-Multiple-Output (MIMO) antenna system with pattern diversity is proposed for 5G N78 band application. All the three ports, which are sequentially rotated by 120°, are integrated together on a circle patch. Each antenna element is fed by a probe and an annular slot etched on the patch which works as a capacitor to counteract the inductance effect introduced by the feeding probe and the nearby shorting posts. A patch-like broadside radiation pattern is generated for each element. By introducing a novel Γ-shaped metal plate for each element, the radiation beam could be tilted and deviate from the z axis by around +30° to suit the diversity application demand. Good isolation is achieved by introducing a metal post between every two ports, which well suppresses the mutual coupling induced by the current between the ports. The working principle of the proposed MIMO antenna is theoretically illustrated in detail and experimentally verified. The Proposed antenna occupies a cylindrical volume of $\pi \times 0.33^2 \times 0.14\ \lambda_0^3$, where λ_0 represents the free space wavelength at the center frequency of the operating band. The measured overlapping bandwidth covers the N78 band (3.3-3.8 GHz) with $|S_{11}| < -10$ dB for the three antenna elements. The proposed antenna offers attractive features including a shared radiation aperture, pattern diversity, good isolation ($\leq$ 20 dB) good gain ($\geq$ 8.2 dBi), low field envelope correlation coefficient value ($\leq$ 0.001), and high radiation efficiency ($\geq$ 74%).

INDEX TERMS 5G new radio (5G NR), multiple-input- multiple-output (MIMO) antennas, pattern diversity, quasi-Yagi antenna.

I. INTRODUCTION

The Yagi-Uda antenna, initially proposed by Uda [1], exhibits the advantages of high front-to-back ratio (FBR), high gain, and directive radiation pattern. Up to now, many designs of quasi-Yagi antennas have been proposed, such as PIFA-driven Yagi [2], helical-driven Yagi [3], patch-driven Yagi [4]–[7], and dipole-driven Yagi [8], [9]. Although their structures are different, they all share the same principle: the parasitic array elements are excited by the active elements by near-field coupling and manipulate the radiation beam.

In modern communication systems, vertical polarization is used more widely than the horizontal polarization. When propagating along the ground, the attenuation of vertically polarized waves is less than that of horizontally polarized waves. In addition, when deployed on a horizontal platform, the receiver and transmitter which are both vertically polarized will not have polarization mismatch no matter how they rotate on the horizontal plane [10]. Therefore, the vertically polarized quasi-Yagi antennas have drawn increasing research interest [3], [7], [10], and [11]. A five-element top-hat monopole Yagi antenna was designed and proposed in [12], achieving vertically polarized endfire radiation pattern at UHF band.

Owing to the fast development of 4G/5G communication, the channel capacity of Sub 6 GHz wireless links is limited by the spectrum resources. Due to the needs to effectively mitigate the multipath fading, and to increase the system capacity and stability, MIMO technology has rapidly become one of the key technologies of the 4G/5G communication [13]. When applying quasi-Yagi antennas to MIMO systems, multiple separated elements are required to provide multiple decoupled transmission signals, which makes the design of compact quasi-Yagi-based MIMO antenna with good

The associate editor coordinating the review of this manuscript and approving it for publication was Santi C. Pavone.

isolation quite challenging. For this reason, only few MIMO antennas based on quasi-Yagi structures have been proposed so far [14]–[19]. The design in [14] achieved dual-polarized waves using dipole-based quasi-Yagi antennas for mm-Wave MIMO terminals. Several loop excited or ring slot excited quasi-Yagi MIMO antennas are proposed in [15]–[17].

Mutual coupling occurs when multiple antennas are integrated in a small area. In order to reduce the mutual coupling, a variety of methods have been proposed. In general, metal walls [20] or metal through holes [21] between antenna elements can reduce the coupling. In addition, the radiator with orthogonal polarization can significantly reduce the spatial coupling for adjacent antenna elements [22], [23]. Decoupling networks such as hybrid coupler [24] and neutralization line [25] have been applied to improve the port isolation in mobile terminals. Moreover, defected ground structure (DGS) [26], electromagnetic bandgap (EBG) structures [27], [28], photonic bandgap structures (PBG) [29], and complementary split-ring resonators (CSRR) [30] have been widely used to reduce the current on the common ground so as to improve the isolation. Besides, it is indicated that the mutual-coupling reduction provided by metamaterial (MTM) and metasurface (MTS) offers a higher level of isolation [31].

In this work, by introducing novel Γ-shaped vertical metal plates, a new structure of three-element vertically polarized quasi-Yagi MIMO antenna with driven elements integrated into one single patch is proposed and successfully developed. Three metal posts are used to achieve good isolation. For each port, a directive beam mode is obtained due to the resonance between the metal plate and driven element. Good pattern diversity for this proposed antenna has been demonstrated. The MIMO antenna working at 5G N78 band shows good efficiency with a compact size.

The paper is organized as follows: the configuration and the working principle of the proposed antenna is introduced in Section II. In Section III, the experimental results are presented and discussed. Section IV concludes this work.

II. ANTENNA CONFIGURATION AND PERFORMANCE ANALYSIS

A. ANTENNA DESIGN

Fig. 1 shows the geometry of the proposed compact vertically polarized quasi-Yagi MIMO antenna. There are three driven elements integrated into a top patch which is printed on a single low-cost F4BME substrate ($\varepsilon_r = 2.2$). The substrate has a thickness of 0.5 mm. The antenna utilizes an air cavity ($H_{air} = 12$ mm, $0.132\lambda_0$ at 3.3 GHz - starting frequency for N78 band) above an aluminum ground plane of 0.5 mm thickness. Three shorting posts (M_1-M_3) are used to obtain good isolation between the ports in 5G-N78 band. Three coaxial SMA connectors are used to feed the MIMO antenna. The interval in terms of rotation angle between every two ports is 120°, which is twice the interval between each port and the adjacent shorting post. A capacitive gap feeding is used to compensate the inductive reactance at each port introduced by the feeding probe and the nearby shorting posts [32].

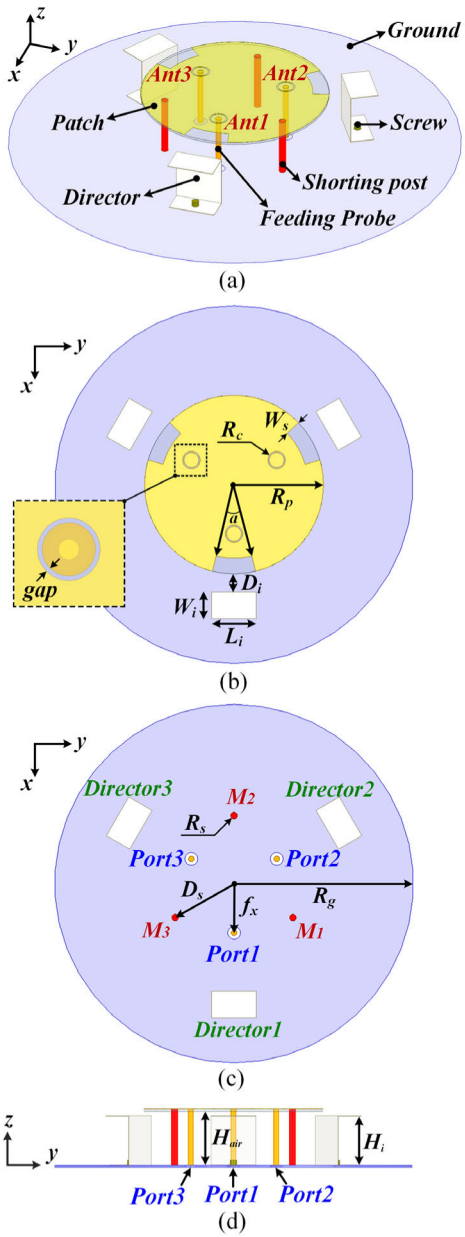

FIGURE 1. Diagram of the proposed MIMO antenna structure: (a) Perspective view; (b) Top view; (c) Bottom view, and (d) Front view.

Three open slots are etched at the edge of the patch to further improve the impedance matching.

A novel and simple Γ-shaped metal plate, which is used as a director with a height of H_i is introduced for each antenna element. A radiation pattern tilted to the direction of the metal plate could be obtained by properly adjusting the size of the metal plate and its distance from the patch. The final optimized parameter values of the proposed MIMO antenna are listed in Table 1.

The design process of the proposed MIMO antenna is divided into the following steps:

1). A circular patch is adopted as a common radiator of the MIMO antenna system, and the three antenna elements are

TABLE 1. Optimal antenna parameter list.

Parameter	Value(mm)	Parameter	Value(mm)
R_p	18	W_i	6
R_g	49	L_i	10
D_s	16	D_i	4
f_x	12	H_i	11
a	12	H_{air}	12
W_s	4	H_1	0.5
R_c	1.1	H_2	0.5
gap	0.2		

fed by three probes from the off-center position symmetrically;

2). Annular slots which works as capacitors are etched on the top patch at the feeding position to compensate the inductive reactance introduced by the feeding probes and the shorting posts;

3). The shorting posts are placed between every two adjacent antenna elements to reduce the mutual coupling;

4). Three open slots are cut at the edge of the patch to improve the impedance matching.

5). Three Γ-shaped metal plates are introduced for each antenna element, which serve as directors to tilt or steer away the radiation beam, so that the pattern diversity is achieved. And the coverage of the antenna system is enhanced.

B. QUASI-YAGI ANTENNA ANALYSIS

When a parasitic element is placed very close to the driven element, an induced electric field with almost equal amplitude and opposite phase would be excited on the parasitic element. The induced electric field is combined with the incident field so that the total tangential field on the conductor is 0 [33], that is:

$$\vec{E}_{parasite} = -\vec{E}_{driver} \tag{1}$$

According to the array theory, the combination of these two elements would lead to a directional endfire radiation pattern. The direction of the endfire radiation beam could be adjusted by tuning the length of the parasitic element. When the electric length of the parasitic element is shorter than the overall radiator's length, it presents capacitance characteristic and acts as a director. When the electric length of the parasitic element is longer than the equivalent resonant length, it presents inductance characteristic and acts as a reflector [34].

Based on the three-port MIMO patch antenna with three shorting posts, a novel Γ-shaped metal plate as a director is designed and introduced for each element, in order to achieve better spatial pattern diversity and obtain good isolation / low

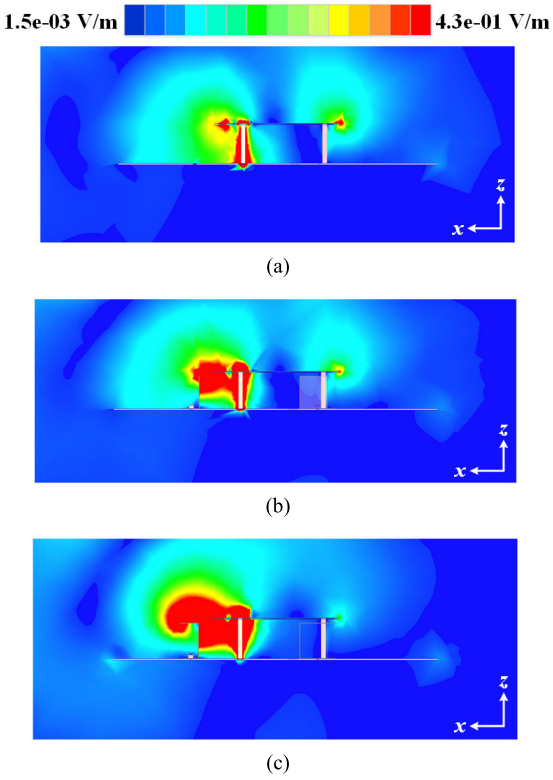

FIGURE 2. E-field distributions at 3.55 GHz in different configurations when Ant. 1 is excited. (a) without three metal plates. (b) with three upright metal plates. (c) with three Γ-shaped metal plates.

envelope correlation coefficient, which is strongly affected by the radiation pattern and polarization of each unit-cell.

In order to illustrate the radiation characteristic of the proposed MIMO antenna more clearly on the basis of the above theory, a detailed analysis is carried out.

First of all, the shape of the director is discussed. The E-field distribution in three cases is given in Fig. 2, where Fig. 2(a) shows the original antenna without any parasitic structure, and Fig. 2(b) shows the antenna loaded with upright parasitic plates, and Fig. 2(c) shows the antenna loaded with Γ-shaped parasitic plates. It is noted that since the three elements of the proposed MIMO antenna are exactly the same, only one element (Port 1) needs to be analyzed here for brevity. The XOZ plane is selected as the observation plane.

When all the three directors are removed as shown in Fig. 2(a), the E-field distribution presents the characteristics of ordinary circular patch antenna (mainly broadside radiation). When three upright directors are introduced as shown in Fig. 2(b), it is noticed that strong E-field is produced at the left side of the patch (In front of Port 1), where the red color seems to be dark. Thus, the radiation beam is tilted from the Z axis towards the X direction. When Γ-shape is used instead of upright shape as shown in Fig. 2(c), the parasitic element can be better excited as a director, which means that the radiation beam would be more inclined to the intended direction (Front side of Port 1).

Secondly, the 'quasi-Yagi' characteristic is analyzed.

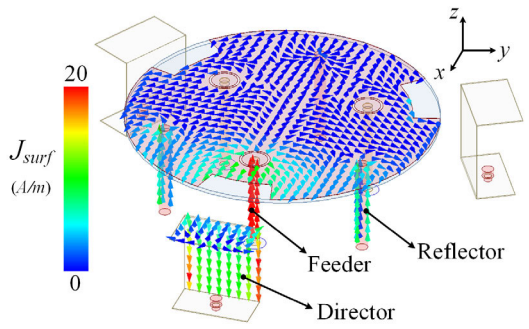

FIGURE 3. Current distribution when Ant1 is working.

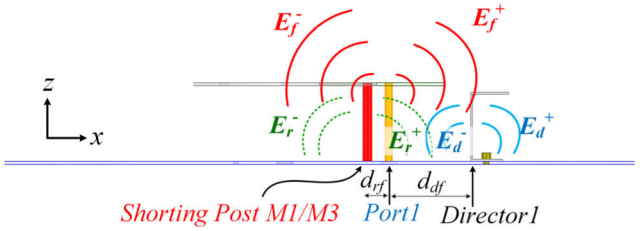

FIGURE 4. Radiation of the vertical part for the proposed antenna.

Fig. 3 shows the current distribution of the proposed MIMO antenna when the Ant1 is working. It can be observed that the vertical parts have strong current distribution which should have contribution to the radiation. Considering the vertical part of the proposed antenna, the three components that make up the Yagi-Uda antenna can be found, that is, the feeding probe represents the active feeder, the Γ-shaped plate serves as the director, and the shorting posts (M1 and M3) and the other non-active antennas can be regarded as the reflector.

According to the superposition principle of waves, the radiation of the vertical part is the superposition of the field generated by the feeder, the director and the reflector. The schematic diagram is shown in Fig. 3. Considering the waves propagating along the +X axis, the electric field they produce at the time $t = 0$ can be approximately expressed as:

$$E_f^+ = A_1 \cos(k_0 x) = \cos(k_0 x) \tag{2}$$

$$\begin{aligned} E_d^+ &= A_2 \cos(k_0(x - d_{df}) + \varphi_{df}) \\ &= 0.8 \cos(k_0(x - d_{df}) - 145^\circ) \end{aligned} \tag{3}$$

$$\begin{aligned} E_r^+ &= A_3 \cos(k_0(x + d_{rf}) + \varphi_{rf}) \\ &= 0.2 \cos(k_0(x + d_{rf}) + 50^\circ) \end{aligned} \tag{4}$$

where E_f^+, E_d^+, and E_r^+ represent the electric field generated by the feeder, the director and the reflector, respectively. The superscript '+' indicates the propagation along the +X axis. The k_0 represents the free space wave number. A_1, A_2 and A_3 represent the amplitudes of the electric field, and assuming that $A_1 : A_2 : A_3 = 1 : 0.8 : 0.2$, which is estimated according to the simulation. The φ_{df} and φ_{rf} represent the phase difference of the director and the reflector with respect to the feeder.

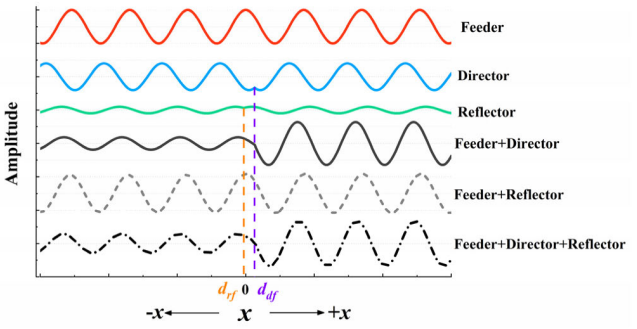

FIGURE 5. Schematic diagram of wave superposition.

Here $\varphi_{df} = -145^\circ$ and $\varphi_{rf} = 50^\circ$ are extracted from the simulation, that is, the phase of current on the Γ-shaped plate lags 145° behind the feeding probe, while the phase of the current on the shorting posts is 50° ahead of the feeding probe. The d_{df} represents the distance between the director and the feeder, and the d_{rf} represents the distance between the reflector and the feeder in the X direction.

For the wave propagating along the −X axis, it can be expressed as:

$$E_f^- = \cos(-k_0 x) \tag{5}$$

$$E_d^- = 0.8 \cos(-k_0(x - d_{df}) - 145^\circ) \tag{6}$$

$$E_r^- = 0.2 \cos(-k_0(x + d_{rf}) + 50^\circ) \tag{7}$$

Fig. 5 shows the numerical calculations according to the equations (2)-(7). The total field can be derived from the superposition of the three components including the field generated by the feeder, the director and the reflector. It can be seen that in the +X direction, the wave increases after superposition, while in the −X direction, the wave weakens after superposition. Consequently, a directional radiation pattern is obtained. Note that the shorting posts has little effect on the total electric field, thus we do not do not emphasize its function as a reflector.

Fig. 6 shows a comparison of the 3D gain patterns for the cases in Fig. 2(a) and Fig. 2(c) at 3.55 GHz when Port 1 is excited, that is, with or without the Γ-shaped plate. It can be seen that the Γ-shaped plate has obvious impact on the radiation pattern as expected. Table 2 shows the comparison of the beam width for the above two cases. It can be concluded that good pattern diversity is achieved by the utilization of the Γ-shaped plate, and the coverage of the antenna system is enhanced accordingly.

For the proposed MIMO antenna, when Port 1 is excited, the 3-D pattern is tilted by around 30° from the broadside (Z direction). Each element of the MIMO antenna proposed in this paper achieves vertical polarization and the three ports are integrated on one radiator to realize the application of multi-input and multi-output, which is different from the horizontally polarized dual-port antenna proposed in [35].

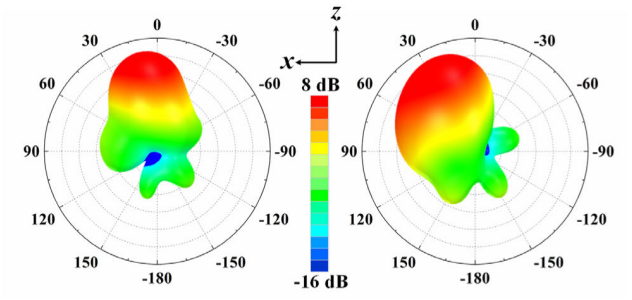

(a) (b)

FIGURE 6. Simulated 3-D radiation patterns at 3.55 GHz for different configurations when Port 1 is excited. (a) without three metal plates. (b) with three Γ-shaped metal plates.

TABLE 2. Comparison of beam width with or without director on XOZ plane when Ant1 is excited.

	Gain	-3dB Beam Width	-6dB Beam Width
Proposed Antenna	7.7dBi	(-3° ~ 61°)	(-13° ~ 90°)
Without Γ-shaped plate	7.3dBi	(-11° ~ 37°)	(-21° ~ 50°)

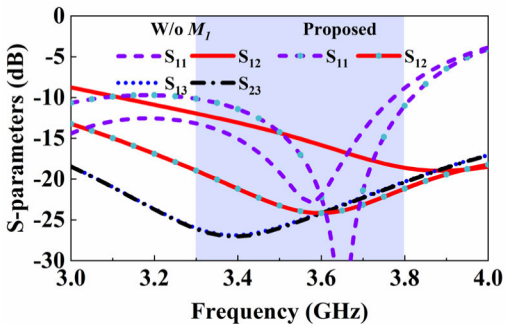

FIGURE 7. Simulated S-parameters of the proposed antenna when M_1 is removed and unremoved.

C. ISOLATION ANALYSIS

For each port in the paper, two symmetrical shorting posts are placed on both sides to ensure good isolation without increasing the size of the antenna. The simulated S-parameters with or without M_1 are shown in Fig. 7. In the desired N78 band, the reflection coefficient is good enough for both cases, while the isolation between the Port 1 and Port 2 is significantly improved after adding M_1. The isolation between port 1 and port 3 seems better without the shorting post M1, yet the $|S_{12}|$ has deteriorated to an unacceptable level.

To further illustrate the role of shorting posts, Fig. 8 shows the surface current distribution on the patch in two cases at a particular phase. It can be found that when only the M_1 is removed, most of the surface current will be coupled from port 1 to port 2. It is conceivable that part of the energy output from Port1 will be transferred to Port2, thus worsening the isolation. In contrast, the shorting post M3 on the left side of the port 1 suppresses the current coupling from port 1 to port 3. Owing to the structural symmetry of the MIMO

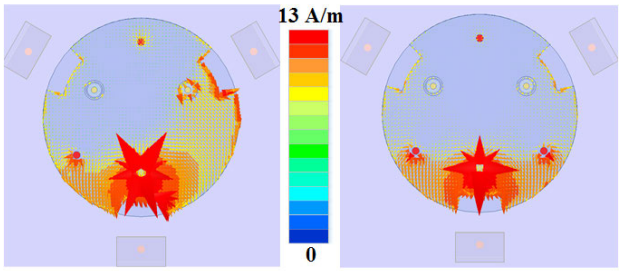

(a) (b)

FIGURE 8. Simulated current distribution for the case with (a) the M_1 not present. (b) the M_1 present.

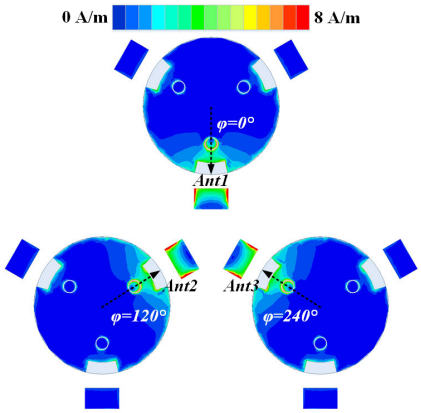

FIGURE 9. Surface current distribution at 3.55GHz for three elements exited, respectively.

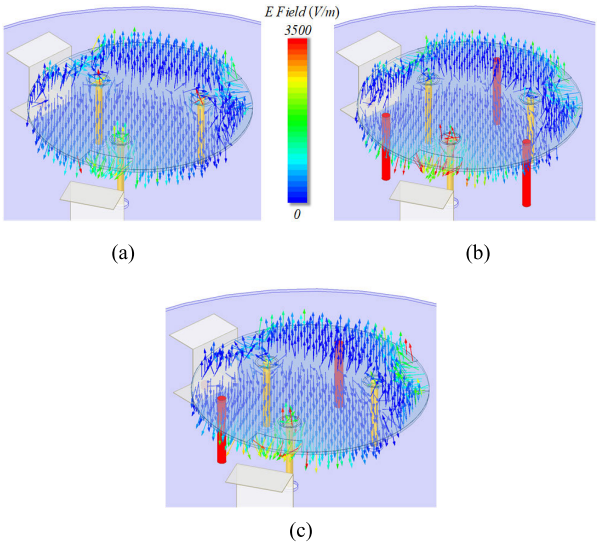

(a) (b)

(c)

FIGURE 10. Simulated E-field distribution for the case with (a) three shorting posts not present. (b) three shorting posts present. (c) the M_1 not present.

antenna, only the study results with M_1 removed are shown for conciseness. M_2 and M_3 play the same role as M_1 due to the symmetry.

Fig. 9 shows the surface current distribution when different element is excited while the remaining ports are matched to 50-ohm load. Note that, the maximum current density

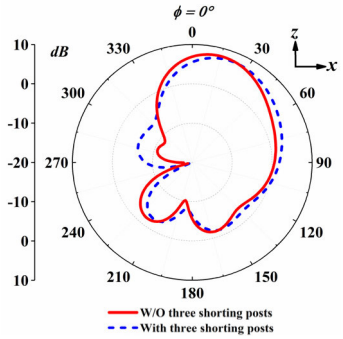

FIGURE 11. The effects on radiation pattern for the case with shorting posts when port. 1 is excited.

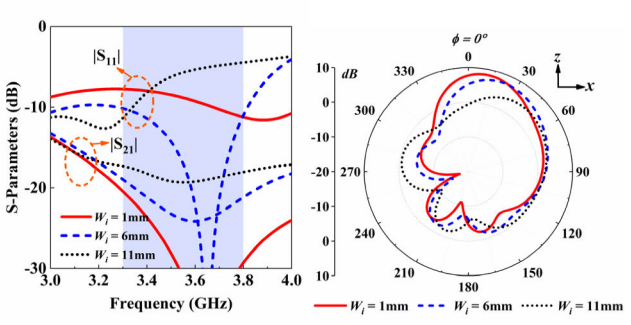

FIGURE 12. The effects on $|S_{11}|$, $|S_{21}|$ and radiation pattern for the cases with different W_i when port. 1 is excited.

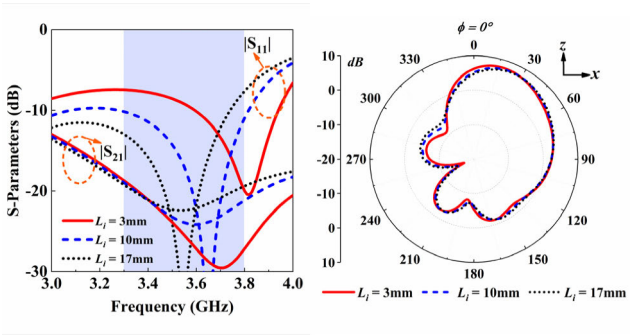

FIGURE 13. The effects on $|S_{11}|$, $|S_{21}|$ and radiation pattern for the cases with different L_i when port. 1 is excited.

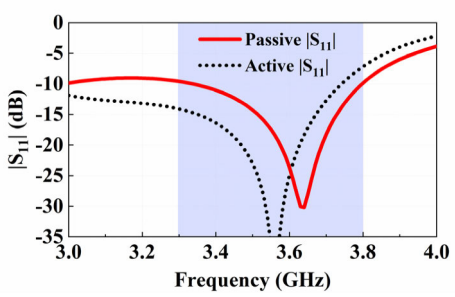

FIGURE 14. Simulated active and passive $|S_{11}|$.

is located between the excited driven element and the Γ-shaped metal plate. Only very weak currents are coupled to other elements due to the existence of three shorting posts, which means that although the three driven elements for the three-element antenna are sharing the same patch, the coupling between every two elements is very weak. Thus, the proposed antenna has the advantage of a compact structure.

When three shorting posts are not introduced, the TM_{11} mode will be excited for each element antenna [18]. Fig 10 shows the E-field distribution on the patch when the Ant 1 is excited. It can be seen that the introduction of three shorting posts have little compact on the operating mode for the MIMO antenna.

Fig. 11 gives the comparison of the simulated radiation pattern in $\varphi = 0°$ plane for Ant. 1 when three shorting posts are introduced and removed, respectively, which shows that the influence for the introduction of shorting posts on the radiation pattern is relatively small.

D. PARAMETRIC ANALYSIS

The effects of the width W_i of the part parallel to the horizontal plane of the metal plate on the antenna performance are studied in Fig. 12. It can be observed that the resonant frequency for port. 1 shifts downward quickly from 3.88 GHz to 3.22 GHz with the pattern deviate from +z axis more obvious as W_i increases from 1 mm to 11 mm, indicates that the existence of the part parallel to the horizontal plane of the metal plate plays a key role in the realization of pattern deflection for each element antenna. Note that the back lobe of the pattern deteriorated with the increase of W_i. In order to achieve good impedance matching and pattern diversity at the same time, $W_i = 6$ mm is selected.

The trend of reflection coefficient versus the length L_i of the part parallel to the horizontal plane of the metal plate is similar to that of W_i, as shown in Fig. 13. In the band below N78, the larger the L_i, the better the impedance matching while the isolation S_{12} is always above −20 dB for different L_i, which also explains why we chose metal plate instead of wire. It can be seen that the radiation pattern is insensitive to the variation of L_i when Ant. 1 is excited. In order to enable the MIMO antenna to work in the N78 band with isolation between each port below −20 dB, $L_i = 10$ mm is selected. $|S_{13}|$ and $|S_{23}|$ are not given in Fig. 12 and Fig. 13, which is due to the symmetry of the MIMO antenna structure.

E. ACTIVE S-PARAMETER

If all the ports are excited simultaneously in a multi-antenna system, the input impedance for the ports may change due to the mutual coupling. Therefore, it is valuable to study its active S parameters. Fig. 14 shows the active $|S_{11}|$ for the proposed MIMO antenna system when the three ports are fed with power of 1 W in the same phase. The impedance matching continues to be acceptable, except that the reflection coefficient is slightly worse at the right edge of the operating band.

III. RESULTS AND DISCUSSION

The MIMO antenna is fabricated and assembled, with a prototype clearly shown in Fig. 15. Here the *S*-parameters is

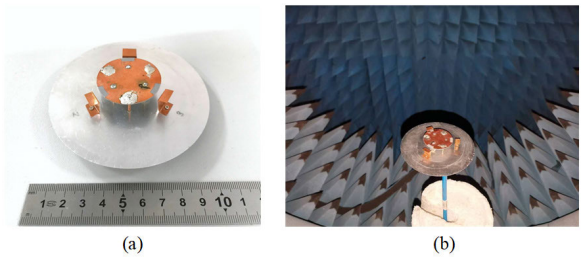

FIGURE 15. (a) Photograph of the prototype. (b) Measurement setup in SATIMO chamber.

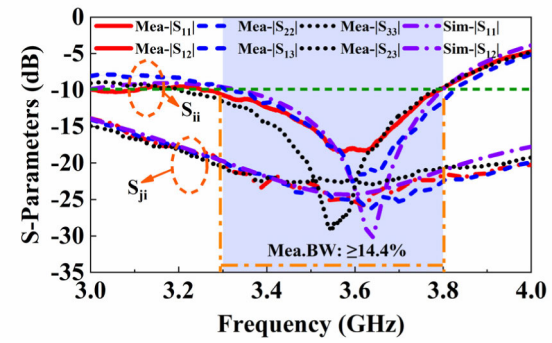

FIGURE 16. Measured and simulated S-parameters for the proposed MIMO antenna ($i \neq j$).

evaluated by R&S ZVB40 VNA (100 kHz-40 GHz), while the radiation performance is tested by a Starlab near-field chamber.

The measured and simulated results for the reflection and transmission coefficients are shown in Fig. 16. The measured and simulated results are in good agreement. It covers the desired N78 band (3.3-3.8 GHz, about 14%) with the overlapping measured bandwidth is 14.4% for the MIMO antenna. In this application, N78 band is the focus and the isolations between the antenna elements in the band are much better. As mentioned above, because of the structural symmetry of the MIMO antenna, only one set of simulated reflection coefficients and transmission coefficients need to be given in Fig. 16. Some frequency deviation for reflection coefficients is observed, which is probably due to the fabrication errors. Note that the MIMO antenna is a non-planar structure. Both the measured and simulated transmission coefficients present good isolation between every two ports, which are lower than −20 dB across 3.3-3.8 GHz.

Fig. 17 shows the simulated and measured gain and efficiency. Simulated gain of Ant. 1 is shown for comparison. In the range of 3.3-3.8 GHz, the measured peak gain is 7.58 dBi for Ant. 1, 8.2 dBi for Ant. 2, and 7.22 dBi for Ant. 3, while the simulated peak gain is 7.6 dBi. The measured efficiency is higher than 74% in the whole band and an average efficiency of 87% is achieved for all the three ports. The simulated and measured results show good consistency. Some small discrepancy is probably due to the fabrication tolerance. Note that the performance of the antenna is relatively sensitive to the size of the director and the distance between each director and driven element.

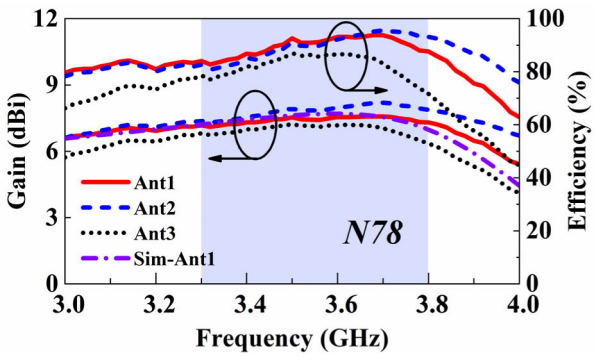

FIGURE 17. Measured and simulated gain and efficiency for the proposed MIMO antenna.

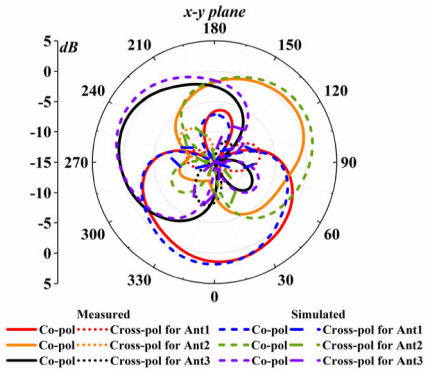

FIGURE 18. Measured and simulated radiation patterns of the MIMO antenna at 3.54 GHz. (a) in XOY ($\theta = 90°$) plane for all elements. (b) in XOZ ($\varphi = 0°$) plane for Ant. 1.

The simulated and measured radiation patterns of the three elements at 3.54 GHz in $\theta = 90°$ (φ cuts) plane and $\varphi = 0°$ plane are compared and presented in Fig. 18. It is seen that from Fig. 18(a) the interval between every two adjacent beams is 120° because the field for Ant. 1-3 reaches maximum at $\varphi = 0°$, $\varphi = 120°$ and $\varphi = 240°$, respectively. It means that the patterns of the three-element antenna are highly uncorrelated. For simplicity, only the measured and simulated side patterns of Ant. 1 are given in Fig. 18(b). It can be seen that the measured result is in good agreement with the simulated result. The element antenna has a good directivity

TABLE 3. Comparison between the proposed antenna and previous works.

Ref	Size (λ_0^2)	Gain (dBi)	Efficiency	BW	Isolation (dB)	ECC	N[*1]	Form
[15]	0.47×0.93	4.3	73%	8%	-12	0.0385	2	Quasi-Yagi.
[18]	0.41×0.41	6.6	88%	23%	-14	0.05	3	Patch.
[37]	0.96×0.96	6	80%	6.3%	-15	0.007	3	Loop.
[38]	0.59×1.18	2.2	49.5%	9.6%	-11.2	0.2	4	Loop.
This work	0.33×0.33	8.2	74%[*2]	14%	-20	0.001	3	Quasi-Yagi.

[*1] N represent the number of the antennas in the applied MIMO systems.

[*2] 74% is the measured lowest efficiency of the proposed MIMO antenna in the working frequency band, and the measured average efficiency is as high as 87% with the highest efficiency is 94%.

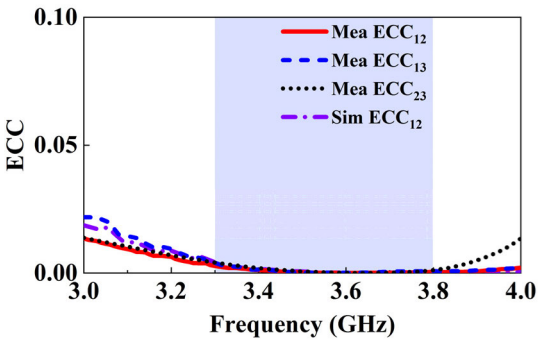

FIGURE 19. Measured and simulated ECC value.

with the maximum radiation direction points to $\theta = 30°$ direction. The above results confirm that the proposed MIMO antenna is a good candidate for pattern diversity applications. For the proposed MIMO antenna system, simulated and measured ECC values were calculated based on the ECC formula shown in [36], and the result is provided in Fig. 19. Only the simulated ECC_{12} is given due to the ECC values of the three cases are the same. It shows that the MIMO antenna has good diversity performance with an average ECC value around 0.001, which is smaller than the standard value of 0.5.

Owing to a good impedance matching and a quasi-Yagi configuration, a relatively high realized gain for each element is obtained with a compact structure. Compared with the previous works as shown in Table 2, our proposed MIMO antenna shows the merits of a higher gain, a wide bandwidth, a novel working principle, and relatively a compact structure.

IV. CONCLUSION

In this work, a three-port vertically polarized MIMO antenna working in the N78 5G band with three Γ-shaped metal plates acting as directors has been proposed and developed. The three driven elements are integrated into a single patch to achieve a compact structure. Strong coupling is generated between each driven element and director resulting in a directional beam, and a relatively high gain compared with conventional MIMO antennas is achieved. It gives the antenna good pattern diversity performance. The MIMO antenna system has a maximum measured gain of 8.2 dBi and good efficiency (>74%) across the band. The proposed antenna is well designed and suited for 5G N78 band applications.

REFERENCES

[1] S. Uda, "Wireless beam of short electric waves," *J. Inst. Electr. Eng. Jpn.*, vol. 46, no. 456, pp. 273–282, Mar. 1926.

[2] R. Bhattacharya, R. Garg, and T. K. Bhattacharyya, "Design of a PIFA-driven compact Yagi-type pattern diversity antenna for handheld devices," *IEEE Antennas Wireless Propag. Lett.*, vol. 15, pp. 255–258, 2016.

[3] Z. Hu, W. Wang, Z. Shen, and W. Wu, "Low-profile helical quasi-Yagi antenna array with multibeams at the endfire direction," *IEEE Antennas Wireless Propag. Lett.*, vol. 16, pp. 1241–1244, 2017.

[4] W.-Q. Deng, X.-S. Yang, C.-S. Shen, J. Zhao, and B.-Z. Wang, "A dual-polarized pattern reconfigurable Yagi patch antenna for microbase stations," *IEEE Trans. Antennas Propag.*, vol. 65, no. 10, pp. 5095–5102, Oct. 2017.

[5] T. Sabapathy, M. Jusoh, R. B. Ahmad, M. R. Kamarudin, and P. J. Soh, "A ground-plane-truncated, broadly steerable Yagi–Uda patch array antenna," *IEEE Antennas Wireless Propag. Lett.*, vol. 15, pp. 1069–1072, 2016.

[6] J. Shi, L. Zhu, N.-W. Liu, and W. Wu, "A microstrip Yagi antenna with an enlarged beam tilt angle via a slot-loaded patch reflector and pin-loaded patch directors," *IEEE Antennas Wireless Propag. Lett.*, vol. 18, no. 4, pp. 679–683, Apr. 2019.

[7] E. Guo, J. Liu, and Y. Long, "A mode-superposed microstrip patch antenna and its Yagi array with high front-to-back ratio," *IEEE Trans. Antennas Propag.*, vol. 65, no. 12, pp. 7328–7333, Dec. 2017.

[8] N. Kaneda, W. R. Deal, Y. Qian, R. Waterhouse, and T. Itoh, "A broadband planar quasi-Yagi antenna," *IEEE Trans. Antennas Propag.*, vol. 50, no. 8, pp. 1158–1160, Aug. 2002.

[9] G. Liu, Y. M. Pan, T. L. Wu, and P. F. Hu, "A compact planar quasi-Yagi antenna with bandpass filtering response," *IEEE Access*, vol. 7, pp. 67856–67862, 2019.

[10] J. Liu and Q. Xue, "Microstrip magnetic dipole Yagi array antenna with endfire radiation and vertical polarization," *IEEE Trans. Antennas Propag.*, vol. 61, no. 3, pp. 1140–1147, Mar. 2013.

[11] Z. Yang, L. Zhang, and T. Yang, "A microstrip magnetic dipole Yagi–Uda antenna employing vertical i-shaped resonators as parasitic elements," *IEEE Trans. Antennas Propag.*, vol. 66, no. 8, pp. 3910–3917, Aug. 2018.

[12] Z. Hu, Z. Shen, W. Wu, and J. Lu, "Low-profile top-hat monopole Yagi antenna for end-fire radiation," *IEEE Trans. Antennas Propag.*, vol. 63, no. 7, pp. 2851–2857, Jul. 2015.

[13] M. S. Sharawi, *Printed MIMO Antenna Engineering*. Norwood, MA, USA: Artech House, 2014.

[14] Y.-W. Hsu, T.-C. Huang, H.-S. Lin, and Y.-C. Lin, "Dual-polarized quasi Yagi–Uda antennas with endfire radiation for millimeter-wave MIMO terminals," *IEEE Trans. Antennas Propag.*, vol. 65, no. 12, pp. 6282–6289, Dec. 2017.

[15] S. S. Jehangir and M. S. Sharawi, "A single layer semi-ring slot Yagi-like MIMO antenna system with high front-to-back ratio," *IEEE Trans. Antennas Propag.*, vol. 65, no. 2, pp. 937–942, Feb. 2017.

[16] S. S. Jehangir and M. S. Sharawi, "A compact single-layer four-port orthogonally polarized Yagi-like MIMO antenna system," *IEEE Trans. Antennas Propag.*, vol. 68, no. 8, pp. 6372–6377, Aug. 2020, doi: 10.1109/TAP.2020.2969810.
[17] S. S. Jehangir and M. S. Sharawi, "A wideband sectoral quasi-Yagi MIMO antenna system with multibeam elements," *IEEE Trans. Antennas Propag.*, vol. 67, no. 3, pp. 1898–1903, Mar. 2019.
[18] K.-L. Wong, C.-M. Chou, Y.-J. Yang, and K.-Y. Wang, "Multipolarized wideband circular patch antenna for fifth-generation multi-input–multi-output access-point application," *IEEE Antennas Wireless Propag. Lett.*, vol. 18, no. 10, pp. 2184–2188, Oct. 2019.
[19] D.-W. Kim and S. Nam, "Systematic design of a multiport MIMO antenna with bilateral symmetry based on characteristic mode analysis," *IEEE Trans. Antennas Propag.*, vol. 66, no. 3, pp. 1076–1085, Mar. 2018.
[20] A. Boukarkar, X. Q. Lin, Y. Jiang, L. Y. Nie, P. Mei, and Y. Q. Yu, "A miniaturized extremely close-spaced four-element dual-band MIMO antenna system with polarization and pattern diversity," *IEEE Antennas Wireless Propag. Lett.*, vol. 17, no. 1, pp. 134–137, Jan. 2018.
[21] M. Alibakhshikenari, B. S. Virdee, and E. Limiti, "Study on isolation and radiation behaviours of a 34 × 34 array-antennas based on SIW and metasurface properties for applications in terahertz band over 125–300 GHz," *Optik*, vol. 206, Mar. 2020, Art. no. 163222.
[22] H. Li, B. K. Lau, Z. Ying, and S. He, "Decoupling of multiple antennas in terminals with chassis excitation using polarization diversity, angle diversity and current control," *IEEE Trans. Antennas Propag.*, vol. 60, no. 12, pp. 5947–5957, Dec. 2012.
[23] S. K. Sharma, L. Shafai, and N. Jacob, "Investigation of wide-band microstrip slot antenna," *IEEE Trans. Antennas Propag.*, vol. 52, no. 3, pp. 865–872, Mar. 2004.
[24] R. A. Bhatti, S. Yi, and S. Park, "Compact antenna array with port decoupling for LTE-standardized mobile phones," *IEEE Antennas Wireless Propag. Lett.*, vol. 8, pp. 1430–1433, 2009.
[25] S.-W. Su, C.-T. Lee, and F.-S. Chang, "Printed MIMO-antenna system using neutralization-line technique for wireless USB-dongle applications," *IEEE Trans. Antennas Propag.*, vol. 60, no. 2, pp. 456–463, Feb. 2012.
[26] C.-Y. Chiu, F. Xu, S. Shen, and R. D. Murch, "Mutual coupling reduction of rotationally symmetric multiport antennas," *IEEE Trans. Antennas Propag.*, vol. 66, no. 10, pp. 5013–5021, Oct. 2018.
[27] M. Alibakhshikenari, M. Khalily, B. S. Virdee, C. H. See, R. A. Abd-Alhameed, and E. Limiti, "Mutual coupling suppression between two closely placed microstrip patches using EM-bandgap metamaterial fractal loading," *IEEE Access*, vol. 7, pp. 23606–23614, 2019.
[28] M. Alibakhshikenari, M. Khalily, B. S. Virdee, C. H. See, R. A. Abd-Alhameed, and E. Limiti, "Mutual-coupling isolation using embedded metamaterial EM bandgap decoupling slab for densely packed array antennas," *IEEE Access*, vol. 7, pp. 51827–51840, 2019.
[29] M. Alibakhshikenari, B. S. Virdee, N. O. Parchin, P. Shukla, K. Quazzane, C. H. See, R. Abd-Alhameed, F. Falcone, and E. Limiti, "Isolation enhancement of densely packed array antennas with periodic MTM-photonic bandgap for SAR and MIMO systems," *IET Microw., Antennas Propag.*, vol. 14, pp. 183–188, Mar. 2019.
[30] A. Ramachandran, S. V. Pushpakaran, M. Pezholil, and V. Kesavath, "A four-port MIMO antenna using concentric square-ring patches loaded with CSRR for high isolation," *IEEE Antennas Wireless Propag. Lett.*, vol. 15, pp. 1196–1199, 2016.
[31] M. Alibakhshikenari, F. Babaeian, B. S. Virdee, S. Aïssa, L. Azpilicueta, C. H. See, A. A. Althuwayb, I. Huynen, R. A. Abd-Alhameed, F. Falcone, and E. Limiti, "A comprehensive survey on 'various decoupling mechanisms with focus on metamaterial and metasurface principles applicable to SAR and MIMO antenna systems,"' *IEEE Access*, vol. 8, pp. 192965–193004, 2020.
[32] Y. Xu, Z. Wang, and Y. Dong, "Circularly polarized slot antennas with dual-mode elliptic cavity," *IEEE Antennas Wireless Propag. Lett.*, vol. 19, no. 4, pp. 715–719, Apr. 2020.
[33] W. L. Stutzman and G. A. Thiele, *Antenna Theory and Design*, 2nd ed. New York, NY, USA: Wiley, 1998, pp. 172–173.
[34] J. D. Kraus and R. J. Marhefka, *Antennas for All Applications*. New York, NY, USA: McGraw-Hill, 2002.
[35] A. Sowmyadevi, P. Mathur, A. R. Chandran, N. Timmons, J. Morrison, and S. Raman, "2.45 GHz pattern reconfigurable antenna for wireless sensor network applications," in *Proc. URSI Asia–Pacific Radio Sci. Conf. (AP-RASC)*, New Delhi, India, Mar. 2019, pp. 1–4.
[36] S. Blanch, J. Romeu, and I. Corbella, "Exact representation of antenna system diversity performance from input parameter description," *Electron. Lett.*, vol. 39, no. 9, pp. 705–707, May 2003.
[37] S.-W. Su, "High-gain dual-loop antennas for MIMO access points in the 2.4/5.2/5.8 GHz bands," *IEEE Trans. Antennas Propag.*, vol. 58, no. 7, pp. 2412–2419, Jul. 2010.
[38] M. Y. Li, Z. Q. Xu, Y. L. Ban, and Z. F. Yu, "Eight-port orthogonally dual-polarised MIMO antennas using loop structures for 5G smartphone," *IET Microw., Antennas Propag.*, vol. 11, no. 12, pp. 1810–1816, 2017.

YIZHEN XU (Graduate Student Member, IEEE) was born in Mianyang, Sichuan, China, in 1996. She received the B.S. degree in the electronic information science and technology from Southwest Petroleum University, Chengdu, China, in 2019. She is currently pursuing the M.S. degree with the University of Electronic Science and Technology of China (UESTC), Chengdu, China. Her research interests include MIMO antennas, electromagnetic antennas, and SIW antennas.

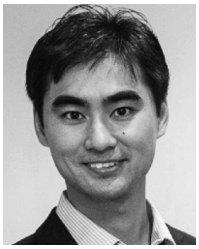

YUANDAN DONG (Senior Member, IEEE) received the B.S. and M.S. degrees from the Department of Radio Engineering, Southeast University, Nanjing, China, in 2006 and 2008, respectively, and the Ph.D. degree from the Department of Electrical Engineering, University of California at Los Angeles (UCLA), in 2012.

From September 2008 to June 2012, he was a Graduate Student Researcher with the Microwave Electronics Laboratory, UCLA. From September 2012 to February 2016, he was a Senior Engineer with the R&D Hardware Department of Qualcomm, San Diego, USA. From February 2016 to December 2017, he was a Staff Engineer with Universal Electronics, Santa Ana. Since December 2017, he has been a Full Professor with UESTC. He has authored over 80 journal and conference papers. His research interests include the characterization and development of RF and microwave components, modules, circuits, different antennas for various applications, acoustic-wave devices, and metamaterials. He was a recipient of the Best Student Paper Award from the 2010 Asia Pacific Microwave Conference, Yokohama, Japan, the Distinguished Expert presented by Sichuan Province and China Government, respectively, and the High Level Innovative and Entrepreneurial Talent presented by Jiangsu Province. He is serving as a reviewer for several IEEE and IET journals, including the IEEE TRANSACTIONS ON MICROWAVE THEORY AND TECHNIQUES and the IEEE TRANSACTION ON ANTENNAS AND PROPAGATION.

SICHAO WEN was born in Linfen, Shanxi, China, in 1996. He received the B.S. degree from Xidian University, in 2018. He is currently pursuing the M.S. degree with the University of Electronic Science and Technology of China. His research interests include wideband antennas, indoor antennas, and miniaturized antennas.

HAILONG WANG was born in 1979. He received the M.S. degree in physical electronics and the Ph.D. degree in electronic and information from the University of Electronics Science and Technology of China, Chengdu, China, in 2004 and 2019, respectively. He is a research-level Senior Engineer and a main member of the Sichuan Province Engineering Research Center for Broadband Microwave Circuit High Density Integration.